Multi-physics methodology for phase change due to rapidly depressurised two-phase flows

M. Chávez-Modena*[a], G. Rubio[a], E. Valero[a], D. Mira[b], O. Lehmkuhl[b]

[a] *ETSIAE-UPM - School of Aeronautics, Universidad Politécnica de Madrid. Plaza Cardenal Cisneros 3, E-28040 Madrid, Spain.,*
Center for Computational Simulation, Universidad Politécnica de Madrid, Campus de Montegancedo, Boadilla del Monte, 28660, Madrid, Spain.
** m.chavez@upm.es*
[b] *Barcelona Supercomputing Center - Barcelona (Spain)*

Abstract

Zonal modeling is a common technique for the numerical certification of fire-extinguishing systems, however it is not valid to simulate the complex physical phenomena that occurs near the agent injection. We present a multi-scale method for the accurate generation of inflow boundary conditions valid for zonal modeling based on the description of the phase change of a rapidly depressurised mist of a fire suppression system. The generation of accurate boundary conditions includes the characterization of the injection of the fire suppression agent from atomization to evaporation and mixing. The multi-scale methodology is based on the use of a high fidelity multiphase conservative level set LES for the characterization of the nozzle to develop an empirical model for primary breakup. Secondly, a low fidelity particle-based method with phase change and unsteady RANS is used for parametric studies. This multi-scale approach requires an affordable computational effort.

The multi-scale methodology is tested in a system consisting of a pressurised fire extinguishing agent (Novec-1230) that is injected into the ambient through a nozzle that produces the atomization of the agent. The accuracy of the developed approach is compared with the experimental data.

Keywords: Multi-physics, Multi-phase flow, Phase change, Novec-1230,

1. Introduction

Fire suppression systems for aircrafts are based on the interruption of the propagation of chain reactions typically found in aeronautical fuels. They historically use hydrofluorocarbons (HFCs) as a fire protection fluid, the most well-known and used one being Halon (R13B1, CFBr3). However, due to their high global warming potentials (GWPs), the industry has been pushed to adopt more environmentally friendly alternatives. Among those, we can find Novec-1230 Fire Protection Fluid [1]. The main difference between Halon and Novec-1230 is, in addition to the lower global potential warming of the latest, its higher molecular weight. As a result, the boiling point at ambient pressure for Novec-1230 is much higher than Halon (215.4 K compared to 322.4 K), and results in different vaporization and dispersion rates. These differences in atomization and evaporation are one of the limiting factors to prevent the direct implementation of Novec-1230 as a new suppression agent, and requires a complete re-design of the system.

Zonal model is a common tool for the numerical certification of fire-extinguishing systems [2, 3, 4, 5, 6, 7]. In the zonal model, an enclosure is divided into zones, each one with approximately uniform properties. These zones interact by exchanging mass and energy, while momentum is typically ignored [8]. The main advantage of zonal models is its low computational cost as they are based primarily on analytical and semi-analytical considerations. The most important disadvantages are [9]: low resolution due to averaging of variables over significant spatial scale, low accuracy for highly unsteady and/or chaotic problems and the necessity of a priori knowledge of the flow structure. As a result, zonal model is not valid to simulate the complex physical phenomena that occurs in the vicinity of the agent injection. To overcome this limitation, in this work, a numerical multi-scale approach is proposed to predict the atomization, the phase change and the spreading of the agent into the compartment, which allow to generate accurate inflow boundary conditions for the zonal model. The multi-scale methodology pro-

posed in this work consists of two steps. The description of the atomization process is captured in the first step by a high fidelity multiphase field modeling. These simulations demand high computational cost as the liquid/gas interface is to be captured, and therefore the computational domain is restricted to the near field of the injector. In this region, the high momentum of the flow and the presence of high concentrations of liquid make the coupling of these results with the zonal model still too complex. Therefore, a secondary set of simulations are defined to describe the phase change of the agent and the mixing with the surrounding gas. This second stage has a much lower computational cost compared to the primary breakup and can be run in a volume of the size of one zone of the zonal model.

The modeling of multiphase flows can be described using Eulerian and Lagrangian methods [10]. In particular, the methodology proposed to characterize the flow discharge with phase change analysed here is based on two different approximations: an Euler–Euler (EE) model for the jet breakup (step one) followed by an Euler–Lagrange (EL) model for the spreading of the agent and phase change (step two). Both methodologies will be described in the following paragraphs.

In EE models, the two phases are treated mathematically as interpenetrating continua. The concept of volume fraction (or void fraction, typically denoted by ϕ) as the fraction of a particular infinitesimal control volume which is occupied by each phase (minimum two), is introduced. Volume fraction is supposed to vary continuously in space and time. Conservation equations for each phase (Navier–Stokes equations) together with physical constitutive relations (usually from experimental correlations) and a partial differential equation for the evolution of the volume fraction are posed. The solution of this set of equations describes the evolution of the flow. Different levels of complexity can be found within the EE models. Among the most simple is the one fluid formulation [11], which defines a single set of momentum equations shared by all phases, while the volume fraction is tracked throughout the domain following a convective equation. The one fluid formulation is used by interface capturing techniques, such as volume-of-fluid

(VOF) [12], level-set (LS) [13, 14] and phase-field (PF) [15, 16, 17] methods. More complex models consider that each of the phases is described by its own density, velocity, temperature and pressure (see for example the Baer and Nunziato model [18, 19]). These models are usually closed with mathematical relations for the interaction between the phases (e.g., drag or pressure relaxation).

On the contrary, EL methods consider that only one of the phases is continuous (Euler), while the other/s is/are dispersed (Lagrange). The continuous Navier–Stokes equations are solved for the Euler phase while the Lagrange particles are tracked (individually or as groups) [20]. Lagrange particles are used to represent objects that fall under the resolution level of the numerical grid. Liquid droplets are one of the most common examples. Two different levels of coupling between the Euler and Lagrange phases are usually considered in EL methods. In the one–way coupling, the dispersed phase is transported by the continuous phase but the latter is not affected by the former. The two–way coupling also considers the effect of the Lagrange into the Euler phase [20].

The level of resolution required to address the whole atomization and vaporization process with an EE high fidelity simulation falls far beyond the current computer capabilities. Therefore, here a multi-scale approach is proposed, where the atomization process (near field - step one) is described by a high fidelity EE simulation, while the vaporization and dispersion of the agent (far field - step two) are simulated with a EL model. This approach is similar to the Eulerian-Lagrangian Spray Atomization (ELSA) model developed in [21]. This model has been successfully applied in the context of spray atomization in diesel engines by several authors [22, 23, 24, 25].

For the near field, the proposed approach accounts for the primary primary breakup of a liquid jet injected into a quiescent air using a high fidelity Large Eddy Simulation (LES) EE model. It is based on an entropy stable conservative level set scheme stabilised with an entropy stable method [26] for the regions where the interface can be resolved, while it includes a subgrid contribution when the slip velocity of the two-phase flow cannot be resolved with the given filter size. For the far field, an EL approxima-

tion is solved which includes a Reynolds Averaged Navier-Stockes (RANS) model for the gas while the liquid is assumed to be dispersed and tracked as individual droplets. This model is only valid to simulate the flow outside the nozzle (after the fire extinction agent has been atomized). A two–way coupled model based on previous works in the simulation of fire suppression systems [27, 28, 29] is used to solve the droplets vaporization in the EL simulation. The coupling between EE and EL models is performed through the definition of the liquid injector. The EE-LES accurate simulation of the atomization process permits the generation of the liquid injection parameters for the EL model. In this work, the EE-LES is performed with the multiphysics code Alya [30], while the EL-RANS simulations are performed with ANSYS–Fluent [31].

The proposed methodology is applied to a generic fire suppression system, made of a nozzle which injects the agent (Novec-1230) into a large compartment. The results are compared with Payri et al.'s experimental work [32]. In the experimental work, Diffuse Backlight Illumination (DBI) [33] and Schlieren techniques [34] are used to distinguish between the liquid and the vapor phases. The experimental visualizations and the measured liquid jet penetration are used to compare and assess the proposed multiscale modeling approach.

The remaining of this work is organised as follows: First, the physical problem is presented in Section 2. Then, Section 3 deals with the numerical methodology. A validation of the multi-physics methodology for a single injector nozzle is performed and compared with the experimental results in Section 4. Finally, in Section 5 the developed methodology is used to study the effect of the injection conditions (temperature and pressure) into the vaporization of Novec-1230.

2. Problem description

An on-board fire extinguisher system usually consists of a bottle and a nozzle, although it can be composed by a complex arrangement of pipes and nozzles [35]. In order to simplify the test rig and facilitate the subsequent

model validation, a pressure-based simplex nozzle oriented in the axial direction was used for the experimental test [32].

The numerical analysis follows the same setup and uses the same nozzle evaluated during the experimental campaign developed by the Universidad Politéctnica de Valencia under the project FireExtinction (Multi-physics methodology for phase change due to rapidly depressurized two-phase flows). The nozzle of Spraying Systems Co. ref. 1/4GG-SS3009 is used (see Figure 1). It has an orifice with a nozzle outlet diameter $d_n = 2$ mm and includes a swirler to add a tangential component to the flow and improve the atomization process. The spray angle obtained in the experimental campaign was $\theta = 30$ deg, which confirms the manufacturer specifications. The design of the test vessel was a prism with an interior volume of 750×750×1500mm, required to avoid any interference of the vessel with the spray development. Four different positions were selected as fields of view, as depicted in Figure 2. Three of them are aligned with the axis of the nozzle, and the fourth one is separated a certain distance from the nozzle to verify the measured spray angle. Two different measurement techniques were used: Diffuse Backlight Illumination (DBI) and the Schlieren techniques. Additional details of the experiments and further description of the setup and experimental procedures can be found in [32].

Figure 1: Spraying Systems Co. Ref. 1/4GG-SS3009 nozzle.

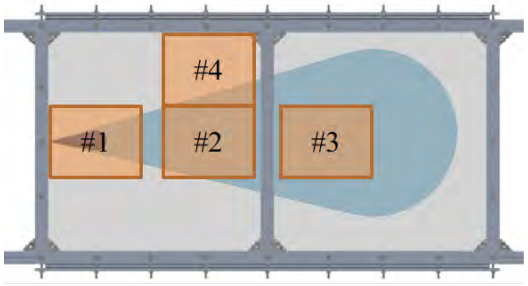

Figure 2: Schematic diagram of the side view of the vessel, showing the four fields of view employed in the measurements.

Novec-1230 at ambient conditions was employed as a fire extinguisher

agent in the experimental test rig. For completeness, the reference properties [1] used in the numerical simulations for this compound are listed in Table 1, where the air properties are also included. The hypothesis of Lewis number equal to one has been made, due to the lack of information on the value of the mass difussivity coefficient (see Table 2).

	Air	**Novec–1230**	
		Liquid	*Vapor*
Molecular Mass, M [kg/mol]	28.96	316.05	
Density, ρ [kg/m^3]	1.164	1670	13.6
Latent heat, L [J/kg]	-	88000	
Viscosity, μ [kg/m s]	1.872E-05	5.24E-04	1.16E-05
Specific heat, c_p [kJ/kgK]	1003.6	1103	891
Thermal conductivity, k [W/m K]	0.0258	0.0588	0.0049
Boiling point , T$_b$ [K]	-	322.2	
Thermal difussivity, α [m^2/s]	2.208E-05	3.321E-08	4.043E-07
Surface tension, σ [N/m]		0.0108	

Table 1: Air and Novec-1230 [1] properties .

The problem under investigation is the description of the atomization, evaporation, and mixing of Novec-1230 at cabin altitude condition (288K and 75000Pa) [7, 36]. The Novec-1230 is injected at 273K into the cargo hold with a mass flow rate $\dot{m} = 0.2347$.

To give some insight into the physical problem considered, Table 2 summarizes the main dimensionless numbers relevant to the problem. Subindexes a and l are used to define the fluid properties of air and liquid Novec-1230 respectively. Besides, d_{32} is the Sauter Mean Diameter (see Eq. 25), d_n is nozzle output diameter, U is the reference velocity, U_p is the reference particle velocity, and D_{lg} the binary diffusion coefficient between the fire extinction agent vapor and the surrounding gas (air).

The Reynolds number shows that the flow can be considered a transition between laminar and turbulent flows. The Weber number is higher than one, meaning that the inertial force is able to break the fluid in an atomization process. A particle with a low Stokes number follows fluid streamlines (per-

Reynolds,	$\mathrm{Re} = \frac{\rho_a \mathrm{U} d_n}{\mu_a}$	1050
Reynolds droplets,	$\mathrm{Re}_d = \frac{\rho_a \|\mathrm{U}_p - \mathrm{U}\| d_{32}}{\mu_a}$	18.15
Weber,	$\mathrm{We} = \frac{\rho_a \mathrm{U}^2 d_n}{\sigma}$	23.03
Stokes,	$\mathrm{St} = \frac{\tau}{\tau_\eta} = \left(\frac{\rho_l d_{32}^2}{18\mu_a}\right)\left(\frac{\mu_a d_n}{\rho_a \mathrm{U}^3}\right)^{-\frac{1}{2}}$	6077
Froude droplets,	$\mathrm{Fr} = \frac{\mathrm{U}_p}{\sqrt{g d_n}}$	90.21
Prandtl,	$\mathrm{Pr} = \frac{c_{p_a} \mu_a}{k_a}$	0.728
Schmidt,	$\mathrm{Sc} = \frac{\mu_a}{\rho_a D_{lg}}$	0.728

Table 2: Formula and approximate values of non-dimensional numbers

fect advection), while a particle with a high Stokes number is dominated by its inertia and continues along its initial trajectory. Therefore, in this problem, the particles trajectory is dominated by their inertia. As a result the turbophoresis effect can be neglected because the Stokes time is much higher than the Kolmogorov time scale [37]. The Froude number shows that the droplets are slightly affected by the gravitational force.

As this multiphysics and multiscale problem can be too expensive to solve with a single framework, a multiscale methodology is proposed to separate the problem from atomization to evaporation and mixing. In the first stage, high-fidelity EE simulation of the flow injection and atomization is used to develop a phenomenological model for primary breakup that can be used as a boundary condition for the EL simulations in a subsequent step. Additionally, a comparison with the experimental data has been performed. Details of this simulation methodology can be shown in the next section.

3. Numerical methodology

As mentioned above, the scale separation is made through the identification of two zones: near and far field. For the near field, the proposed approach studies the primary atomization of a liquid jet injected into air using a high-fidelity Large Eddy Simulation (LES) EE model. For the far field, a Reynolds Averaged Navier-Stokes (RANS) EL approximation is solved, which includes a Eulerian description for the gas, while the liquid is assumed to be dispersed and tracked as individual droplets. Both models are coupled

through the boundary condition (definition of the injector) for the EL model obtained from the EE model.

3.1. Near field: Euler-Euler model

The near field corresponds to the internal flow of the nozzle and the region outside the nozzle where the primary breakup occurs. No phase change is considered here. In this work, the proposed Euler–Euler (EE) approach is considered to study the primary breakup of Novec-1230 in air using a LES-based methodology with an entropy stable conservative level set method [38]. This model is implemented in Alya [30] solver.

The modeling approach includes an extension of the conservative level set equation stabilised with an entropy stable method [26] for the regions where the interface can be resolved, while it includes a subgrid contribution when the slip velocity of the two-phase flow can not be resolved with the given filter size [39].

The system of equations is given by the conservation of momentum $\rho\mathbf{u}$, liquid volume fraction ϕ, and liquid/gas interface Σ in the incompressible limit. The system is closed by the equation of state for a liquid/gas mixture given by $\rho = \phi\rho_l + (1-\phi)\,\rho_g$, where the density of the gas ρ_g and liquid ρ_l phases can be obtained by equations of state for gas and liquid respectively, but are assumed to be constant in this study.

The liquid/gas interface density Σ represents the quantity of liquid/gas interface per unit of volume, and it is used to provide the characteristics and sizes of the liquid droplets in the dense part of the spray. A Favre-averaged notation is used to describe the governing equations in LES.

A decomposition of $\overline{\Sigma}$ following Chesnel at al. (2011) [39] is used and the subgrid surface density Σ' that evolves similar to $\overline{\Sigma}$ is solved instead. This separation is based on the existence of a minimum surface density Σ_{min} due to the presence of liquid and a subgrid surface density Σ' that evolves similar to $\overline{\Sigma} = \Sigma_{min} + \Sigma'$, where Σ_{min} is obtained from empirical correlations based on DNS [39] and given by:

$$\Sigma_{min} = \frac{\alpha}{\overline{\Delta}}\sqrt{\overline{\phi}\left(1-\overline{\phi}\right)}, \tag{1}$$

with $\overline{\Delta}$ being a characteristic length scale (filter size in standard LES with implicit filtering) and $\alpha = 2.4$. Therefore, the transport equation for the liquid-gas interface can be expressed in terms of Σ' rather than $\overline{\Sigma}$.

The complete set of governing equations reads:

$$\frac{\partial(\overline{\rho}\overline{\mathbf{u}})}{\partial t} + \nabla \cdot \overline{\rho}\overline{\mathbf{u}}\overline{\mathbf{u}} + \nabla \overline{p} = \nabla \cdot \left[\mu(\nabla \overline{\mathbf{u}} + \nabla \overline{\mathbf{u}}^T)\right] + \sigma k \mathbf{n} \delta_\Gamma - \nabla \cdot \tau_{ij}, \quad (2)$$

$$\nabla \cdot \overline{\mathbf{u}} = 0, \quad (3)$$

$$\frac{\partial \overline{\phi}}{\partial t} + \nabla \cdot (\overline{\mathbf{u}}\overline{\phi} - \nu(\frac{(\overline{\phi} - \phi_L)(\phi_R - \overline{\phi})}{h||\nabla \overline{\phi}||})^+ \nabla \overline{\phi}) = -\nabla \cdot \tau_\phi, \quad (4)$$

$$\frac{\partial \Sigma'}{\partial t} + \nabla \cdot (\overline{\mathbf{u}}\Sigma') = \nabla \cdot (\Sigma' (\overline{\mathbf{u}} - \mathbf{u}_\Gamma)) + \dot{\Sigma}_{int}, \quad (5)$$

where ν is the minimum between the upwind viscosity and the entropy stable entropy and μ the dynamic viscosity. The filtered velocity is $\overline{\mathbf{u}}$, $\overline{p}$ is the filtered pressure and $\tau_{ij} = \overline{\mathbf{u}\mathbf{u}} - \overline{\mathbf{u}}\overline{\mathbf{u}}$ is the subgrid-scale (SGS) stress tensor. The SGS stresses tensor τ_{ij} is determined by the use of the Boussinesq approximation with $\tau_{ij} = \mu_t(\nabla \overline{\mathbf{u}} + \nabla \overline{\mathbf{u}}^T)$, while the eddy viscosity μ_t is computed following the closure proposed by Vreman [40]. The turbulent flux, τ_ϕ, and the slip velocity $\Sigma' (\overline{\mathbf{u}} - \mathbf{u}_\Gamma)$ are both modelled using a gradient assumption closure [39, 41]. The source term $\dot{\Sigma}_{int}$ represents the production/destruction of surface density by the mean shear, turbulence and liquid structure interactions [39] and is modeled by:

$$\dot{\Sigma}_{int} = \frac{\overline{\Sigma}}{\tau_b}\left(1 - \frac{\overline{\Sigma}}{\Sigma_{crit}}\right). \quad (6)$$

The characteristic time scale τ_b can be related to a turbulent time scale as in the dense zone of the spray most of the liquid structures break-up and coalescence by turbulence [39] and the same hypothesis is considered here.

The equilibrium value of surface density Σ_{crit} is obtained from a critical Weber number expressed in terms of the balance of turbulent kinetic energy and takes the form of:

$$\Sigma_{crit} = \Sigma_{min} + \overline{\phi}\left(1 - \overline{\phi}\right)\frac{\overline{\rho}k}{\sigma \mathrm{We}_{\mathrm{crit}}}. \quad (7)$$

Equation (7) is obtained for isothermal flows assuming the surface energy is locally in dynamic equilibrium with the local kinetic energy, and without including the viscous stresses [41].

The governing equations are solved using linear finite elements. The spatial discretization is based on a low dissipation finite element method with an explicit algorithm of the fractional step to solve the velocity/pressure coupling [42] and an entropy stable conservative level set [26] for the volume fraction equation. The main difference with Guermond work [26] is the use of a cell-based viscosity instead of an edge-based version. This approach results in a second-order spatial discretization for both momentum and volume fraction. While the temporal discretization is based on a third-order energy preserving Runge-Kutta scheme for the two equations.

3.2. Far field: Euler–Lagrange model

The far field focuses on the description of the vaporization process, which is solved through a Euler–Lagrange model (EL). In the EL approximation, the multiphase flow problem is solved with a Eulerian description of the gas phase, while the liquid is assumed to be dispersed and it is tracked with a Lagrangian Particle Tracking (LPT) method. This model is applied to the dilute part of the spray and is used to simulate the flow outside the atomiser (after the fire extinction agent has been atomized). The model considers a modification of the Euler solver to take into account the Lagrange (drops) part and an individual evolution of droplets. The LPT approach requires the definition of an appropriate spray injection, which is obtained from the EE approach for Novec-1230 air injection at atmospheric pressure.

3.2.1. Euler solver

In this section, the RANS modeling framework for the gas phase of the EL method is presented with the coupling terms coming from the liquid phase of the LPT method.

Momentum equation:

$$\frac{\partial(\rho\mathbf{u})}{\partial t} + \nabla\cdot\rho\mathbf{u}\mathbf{u} + \nabla p = \mathbf{f}_b + \rho\mathbf{g} + \nabla\cdot\left[(\mu+\mu_t)(\nabla\mathbf{u}+\nabla\mathbf{u}^T)\right], \quad (8)$$

where now ρ refers to the gas density and $\mathbf{u}$ its the time averaged velocity, p is the time averaged pressure (obtained from the incompressibility condition

$\nabla \cdot \mathbf{u} = 0$), $\mathbf{f}_b$ represents the momentum transferred from particles to the gas (see Eq. 14), μ is the kinematic viscosity of the gas mixture and $\mathbf{g}$ is the gravitational acceleration. Similar to the LES equations the turbulent stresses are modeled using an eddy-viscosity approach, in particular, μ_t is the turbulent viscosity coming from the Realizable k-ϵ two-equation RANS model.

Energy equation:

$$\frac{\partial(\rho E)}{\partial t} + \nabla \cdot [\mathbf{u}(\rho E + p)] = \nabla \cdot \left[(k + \frac{\mu_t}{c_p Pr_t}) \nabla T \right] + q_b, \tag{9}$$

where the time averaged energy E is based on the specific heat and the temperature T, k is the thermal conductivity , q_b represents the energy transferred from the particles to the gas (see Eq. 20), c_P is the heat capacity at constant pressure and Pr_t is the turbulent Prandtl number.

Species transport equation: An additional transport equation describing the time averaged mass fraction of the fire extinction agent (vapor) in the gas phase is used to track the mixing fields between the agent and the air. It reads as:

$$\frac{\partial(\rho Y_1)}{\partial t} + \nabla \cdot (\rho Y_1 \mathbf{u}) = \nabla \cdot (\rho D_{lg} + \frac{\mu_t}{Sc_t} \nabla Y_1) + \dot{m}'''_{evap}, \tag{10}$$

where ρ is the density of the air, Y_1 is the time averaged mass fraction of fire extinction agent vapor in the gas, D_{lg} is the diffusion coefficient of fire extinction agent vapor in the gas and $\dot{m}'''_{evap}$ is the source term due to evaporation (see Eq. 19) and Sc_t is the turbulent Schmidt number.

3.2.2. Lagrange solver

The LPT solver accounting for momentum, heat, and mass transfer is described here. This approach is defined using "superdroplets" or parcels, which represent a group of droplets with the same diameter and thermophysical properties [27]. This approach can reduce the computational cost of the simulation, specially when many droplets are to be used.

Momentum equation:

$$\frac{d\mathbf{u}_p}{dt} = \mathbf{g} - \frac{1}{2}\frac{\rho C_d A_{p,c}}{m_p}(\mathbf{u}_p - \mathbf{u})|\mathbf{u}_p - \mathbf{u}|, \tag{11}$$

where $\mathbf{u}_p$ is the particle velocity, $\mathbf{g}$ the gravitational acceleration, C_d its drag coefficient (function of its Reynolds number), $A_{p,c}$ the particle cross–sectional area and m_p the particle mass. Gas velocity, $\mathbf{u}$, and gas density, ρ, are obtained from the Euler part of the solver. The momentum equation solved by ANSYS–Fluent takes into account the buoyancy effects, which are negligible for liquid droplets moving through the air. Being the velocity of the particles known, the particle position, $\mathbf{x}_p$, is determined from the equation, $\frac{d\mathbf{x}_p}{dt} = \mathbf{u}_p$. Based on a sphere, the drag coefficient is computed as:

$$C_d = \begin{cases} 24/Re_D & Re_D < 1 \\ 24(0.85 + 0.15Re_D^{0.687})/Re_D & 1 < Re_D < 1000 \\ 0.44 & 1000 > Re_D \end{cases} \tag{12}$$

with

$$Re_D = \frac{\rho|\mathbf{u}_p - \mathbf{u}|2r_p}{\mu(T)}, \tag{13}$$

where $\mu(T)$ is the dynamic viscosity of air at temperature T and r_p the particle radius.

By summing the forces transferred from each particle in a grid cell and dividing by the cell volume, V, the momentum transferred from particles to the gas (see Eq. 8) is obtained:

$$\mathbf{f}_b = \frac{1}{V}\sum\left[\frac{\rho}{2}C_d A_{p,c}(\mathbf{u}_p - \mathbf{u})|\mathbf{u}_p - \mathbf{u}|\right]. \tag{14}$$

Energy and mass balance equations: To account for droplet heating and evaporation, the energy and mass balance equations for the droplet need to be solved. The evaporation is mass transfer controlled as the ambient temperature and the injected liquid are under the boiling temperature of Novec-1230 (322.2K) in all experiments considered. In fact, the evaporation rate is a function of the liquid equilibrium vapor mass fraction, Y_2, the local

gas phase vapor mass fraction, Y_1, the (assumed uniform) droplet temperature T_p and the local gas temperature, T. The temperature distribution within the droplet may be ignored for problems where the Biot number is less than 0.1 [43, 44]. For our flow condition, the Biot number is:

$$\mathrm{Bi} = \frac{k_h}{k_p}\frac{r_p}{3} \approx 0.1 \tag{15}$$

where k_h is the heat transfer coefficient, k_p is the thermal conductivity of the particle and r_p the radius of the particle. Although the criterion for a lumped system is not exactly met, we consider that the uncertainty introduced by the uniform temperature assumption is reasonable.

The mass and energy transfer can be described by the following set of equations:

$$\frac{dm_p}{dt} = k_m A_{p,s} \rho \ln(1 + B_m), \tag{16}$$

$$\frac{dT_p}{dt} = \frac{1}{m_p c_p}\left[A_{p,s} k_h (T - T_p) + \frac{dm_p}{dt} h_v\right], \tag{17}$$

where B_m is the Spalding mass quantity given by:

$$B_m = \frac{Y_2 - Y_1}{1 - Y_2}. \tag{18}$$

Here, m_p is the mass of the droplet, $A_{p,s}$ the surface area of the liquid droplet, k_m the mass transfer coefficient (to be discussed below), ρ the gas density, c_p the liquid specific heat, k_h the heat transfer coefficient between the droplet and the gas and h_v the latent heat of vaporization of the liquid.

Again, by summing for all particles in a cell we get the source term for the advection equation, see Eq.10, which is:

$$\dot{m}'''_{evap} = -\frac{1}{V}\sum \frac{dm_p}{dt}, \tag{19}$$

where V is the cell volume. As far as the source term for the energy equation, see Eq.9, it reads:

$$q_b = \frac{1}{V}\sum \left[A_{p,s} k_h (T_p - T) - \frac{dm_p}{dt}(h_v + h_l)\right], \tag{20}$$

where h_l is the liquid specific enthalpy, and h_v is the latent heat of vaporization of the liquid.

To evaluate Eq. 16, the vapor mass fraction of the extinction agent in the gas Y_1 is obtained from Eq. 10 while the liquid equilibrium vapor mass fraction is obtained by assuming chemical equilibrium between phases defined by the Clausius-Clapeyron equation:

$$X_2 = \exp\left[\frac{h_v W}{R}\left(\frac{1}{T_b} - \frac{1}{T_p}\right)\right], \tag{21}$$

$$Y_2 = \frac{X_2}{X_2(1 - W_a/W) + W_a/W}, \tag{22}$$

where X_2 is the equilibrium vapor volume fraction, W is the molecular weight of the gaseous species (fire extinction agent), W_a is the molecular weight of air, R is the universal gas constant and T_b is the boiling temperature of the fire extinction agent at standard atmospheric pressure.

Mass and heat transfer coefficients between liquid and gas are described with analogous empirical correlations. The mass transfer coefficient, k_m is described by:

$$k_m = \frac{\mathrm{Sh} D_{lg}}{L}; \quad \mathrm{Sh} = 2 + 0.6\mathrm{Re}_D^{\frac{1}{2}}\mathrm{Sc}^{\frac{1}{3}}, \tag{23}$$

where Sh is the Sherwood number, D_{lg} the binary diffusion coefficient between the fire extinction agent vapor and the surrounding gas (air), L is a length scale (equal to the droplet diameter), Re_D is the Reynolds number of the droplet (based on the droplet diameter, D, and the relative air-droplet velocity) and Sc is the Schmidt number ν/D_{lg} ($\nu = \mu/\rho$ is the kinematic viscosity).

An analogous relationship exists for the heat transfer coefficient:

$$k_h = \frac{\mathrm{Nu} k}{L}; \quad \mathrm{Nu} = 2 + 0.6\mathrm{Re}_D^{\frac{1}{2}}\mathrm{Pr}^{\frac{1}{3}}, \tag{24}$$

where Nu is the Nusselt number, k is the thermal conductivity of the gas, and Pr is the Prandtl number.

It should be noticed that the exchange of mass and energy between liquid droplets and the surrounding gases is computed droplet by droplet (or

parcel by parcel). After the temperature of each droplet is computed, the appropriate amount of vaporised liquid is added to the given mesh cell, and the cell gas temperature is balanced based on the energy exchange between the droplet and the surrounding [29].

3.3. Coupling between near and far fields

As mentioned before, none of the previous approaches is well suited to solve efficiently the complete physical phenomena (discharge, atomization and vaporization of the fire suppression agent). Therefore, a multi-scale approach is proposed to solve this problem. First, the nozzle internal flow and the primary breakup (near field) is solved using the high fidelity EE simulation, and second, the heating, vaporization, mixing and dispersion of the agent (far field) are simulated with the EL model.

For illustration, Figure 3 represents the modelization of the problem with these two approaches. The complete domain is split in two overlapping regions: on the one hand, the blue box represents the two–phase LES solver domain, where the atomization process occurs. On the other hand, the red dashed box represents the EL solver domain where the liquid can be considered dispersed and the phase change occurs. The coupling of the two sets of simulations is addressed by the definition of the liquid injection parameters for the EL model [10]. In this work, the high-fidelity simulation of the atomization process obtained with the EE-LES model will be processed and used (see green line in Figure 3) as a liquid injection for the computation of the EL-RANS model in the far field domain.

The main parameter controlling the transition from the two–phase Euler to the Euler–Lagrange model is the liquid volume fraction, ϕ, that represents the volume occupied by the liquid with respect to the cell volume. We consider that the transition is complete when the liquid volume fraction becomes lower than 0.1. This quantity is a compromise between the computational cost and resolution of the EE model, which satisfies the hypothesis that most of the liquid is already atomized and can be represented by spherical droplets.

This void fraction defines a transition surface composed of the computational cells that form the border with the dense zone (i.e., the zone where

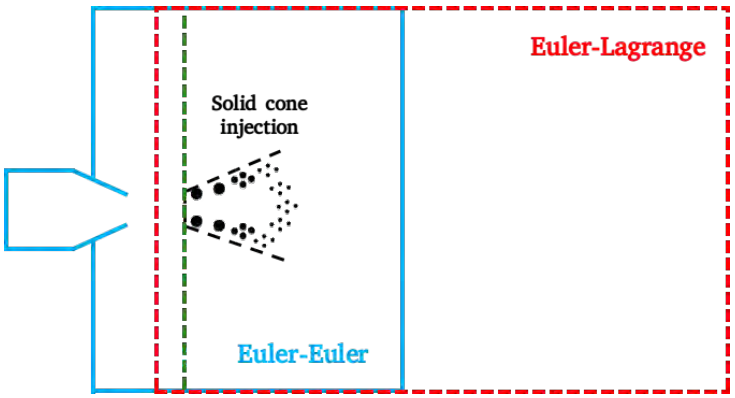

Figure 3: Sketch of the coupling between EE and EL models

the liquid volume fraction is greater than 0.1). Using the interphase surface density and the liquid volume fraction, the Sauter mean diameter (SMD), d_{32}, (see Eq. 25) can be obtained [21] and used to obtain the particle size distributions and statistics of the atomization process. In this work, the mean SMD $< d_{32} >$ is obtained from the time-averaged local SMD (see Eq. 26).

$$d_{32} = \frac{6\phi}{\Sigma}, \tag{25}$$

$$< d_{32} >= \frac{\int_{t_0}^{t} d_{32}(\vec{x}, t)dt}{\Delta t}. \tag{26}$$

From the mean SMD $< d_{32} >$, the number of droplets generated in a given volume is obtained from the mass conservation equation:

$$n_{drop} = \frac{\phi V_{cell}}{\frac{\pi}{6} d_{32}^3}, \tag{27}$$

where V_{cell} is the volume of each transitional cell. Finally, the EL simulation uses an extended domain and injects the particles with the droplet diameter and velocity values extracted from the transition zone using a planar circle injection. This methodology is proved in the following section with the validation in a single injector nozzle.

4. Validation

This section is divided in two parts. First, the Euler-Euler simulation, which includes the study of the transient and steady state agent injection and atomization. A comparison with the experimental data in terms of liquid penetration is also performed with the nozzle partially filled or empty of the agent. In a second step, a simple phenomenological injection model is developed using information from the liquid phase of the EE simulation. *Introducir la descripcion experimental con los fields view*

4.1. Continuous droplet model (Euler-Euler)

The main purpose of this section is twofold. First, the comparison of the high-fidelity results with the available experimental data (transient and steady state), ensuring that the modeling approach is representative of the experimental conditions, and second, the generation of a phenomenological spray model that can be used to validate the low-fidelity simulations.

The operating condition that is used for the development of the phenomenological spray model and used for the coupling Eulerian-Lagrangian is the steady state flow condition reached for a fixed flow rate during the nominal operating point of the injection.

4.1.1. Numerical Setup

The unstructured mesh employed to simulate the injector system is composed by 81.6 million tetrahedrons that include the internal flow in the nozzle and the discharged atmosphere. Three levels of refinement are considered to characterize the internal flow and the near field after the expansion, the jet penetration up to 15D (being D=2mm, the diameter of the nozzle) and the surrounding air with a mesh resolution of 0.1, 0.3 and 1.5 mm respectively (see Figure 4).

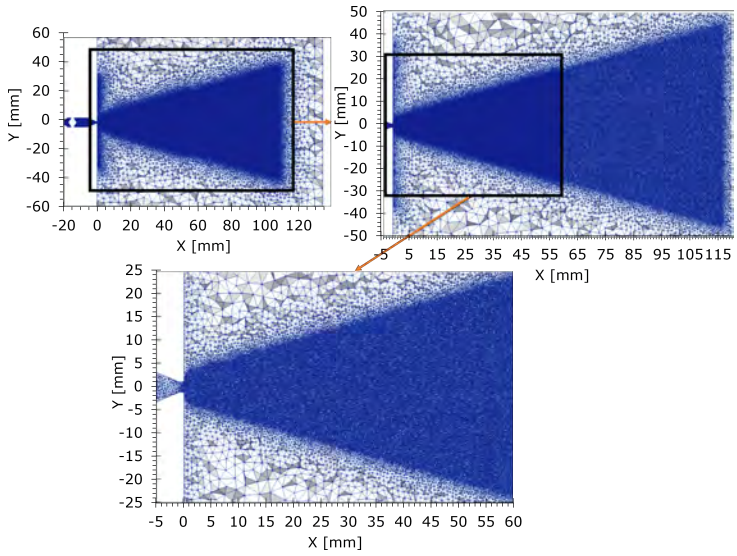

Figure 4: Mesh with three levels of refinement

Regarding the boundary conditions at the inlet, the experimental transient curve of the mass flow rate is imposed, no slip boundary conditions are enforced in the injector system walls, and a pressure-based outlet conditions are fixed in the other surfaces. The effect of the initial condition for the liquid phase is assessed in detail in the next section.

The current mesh resolution shows a good compromise between accuracy and computation time in the prediction of the volume fraction and the velocity field, however, is still far from DNS resolution. To run this time-resolved simulation, 1920 CPUs from Marenostrum IV have been used in each run. A final transient database of 0.5Tb has been obtained to build the phenomenological spray model.

4.1.2. Transient state

The initial analysis considers the numerical and experimental comparison of the spray penetration at the initial stages of the jet discharge. The experiments were conducted by Payri et al. [32]. The comparison is shown in Figure 5. It evidences the importance of the degree of filling of the injector nozzle (see Figure 6). This injector is characterized by a large volume, which after each discharge gets partially filled with liquid. The mixing of fuel and

air inside the injector introduces a delay in the penetration of the jet, which is associated with the time required to discharge all air. Unfortunately, there is no experimental information on the actual level of Novec-1230 in the injector nozzle for each of the different experimental runs, so three different levels of filling, 100%, 50% and 30%, are shown and compared to the experimental data using two different visualization techniques. The effect of the initial condition is clearly observed. Despite this uncertainty, a good agreement is observed between the numerical and experimental results in terms of spray penetration correlation, which suggests that the liquid filling in the nozzle only introduces a delay on the injection that is recovered once the air is ejected. For illustration, the evolution of the injector nozzle with the velocity and fraction of volume is depicted in Figure 6 considering the nozzle is filled with 50% of its volume.

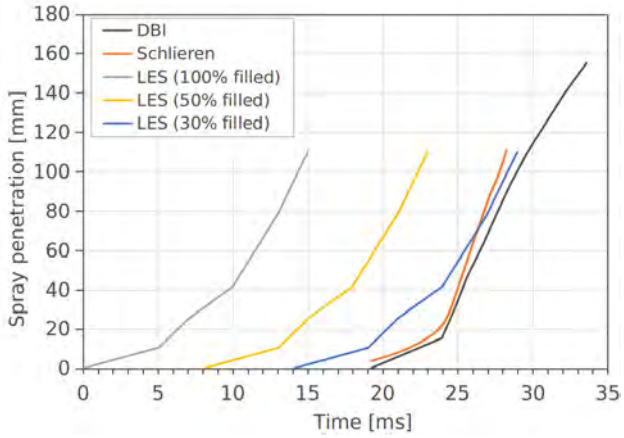

Figure 5: Novec-1230 spray penetration for the transient experiment, LES vs Experimental data

As observed in Figure 5, the penetration trend changes from a parabolic-like profile to a straight line-like when the spray reaches the steady state. At this stage, the pressure stabilises and the injection mass flow rate is constant.

This transition is clearly observed in the experimental sequence depicted in Figure 7. From the start of injection until approximately 12ms (Figure 7d), there is a narrow liquid core due to the acceleration of the fluid from the injection system pipes (parabolic penetration), pushed out through the

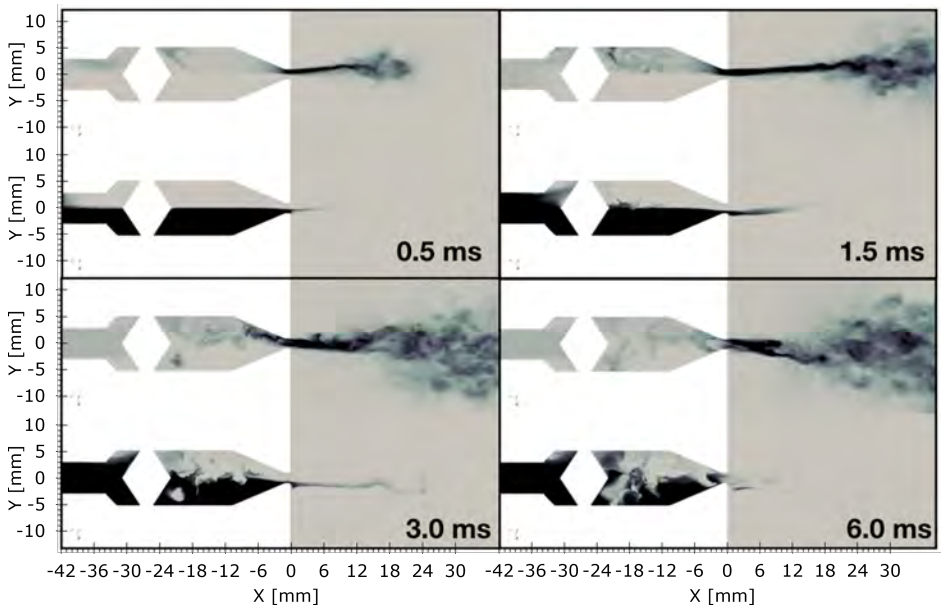

Figure 6: Early transient evolution of both velocity (top) and fraction of volume (bottom) with a 50% of the injector volume filled by Novec-1230 as initial condition

nozzle that primes the swirler. After this delay, the swirl becomes effective with the expected flow rate and provides the spray with a significant azimuthal velocity that promotes the atomization process. Then, the steady state is reached, see Figure 7e. It can be seen that this transient behavior of the injector during the early stages is not relevant during the continuous operation of the atomizer.

The qualitative comparison between the experimental results with DBI images and the evaporated Novec-1230 distribution is shown in Figure 8. Despite the differences in the injection curve between experiments and simulations, the steady state of the discharge processcan be distinguished. The results indicate a good qualitative agreement in terms of spray angle and Novec-1230 distribution.

During stable operation, the liquid jet core penetrates to 30 deg spray angle for about 10D and the jet breaks up into filaments and large droplets with an extension larger than the refinement region of 15D as shown in Fig-

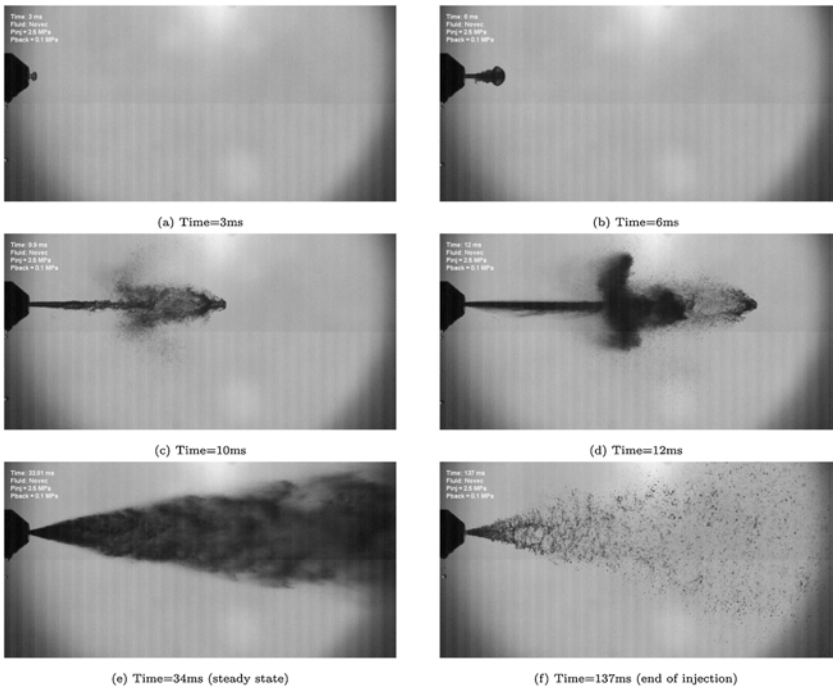

Figure 7: Experimental spray development of Novec-1230 injection at 2.5 MPa of injection pressure and ground level ambient conditions (298 K and 0.1 MPa). Extracted from [32]

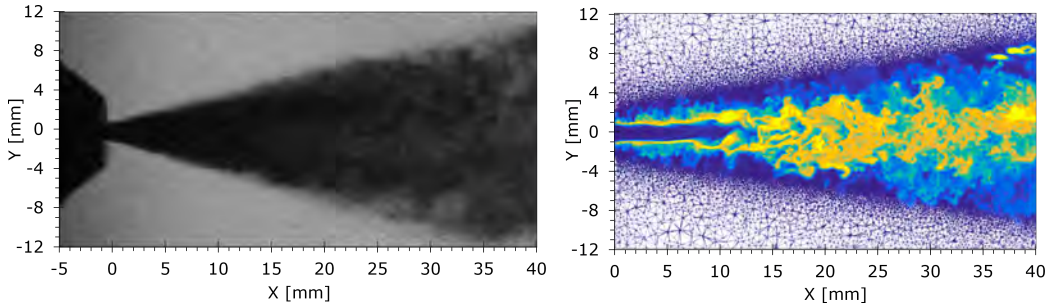

Figure 8: Comparison of DBI images (left) and LES simulations (right) of the Novec-1230 spray at steady state of the discharge process on Field View #1.

ure 9.

The dynamics of the spray can be visualised by an iso-contour of the

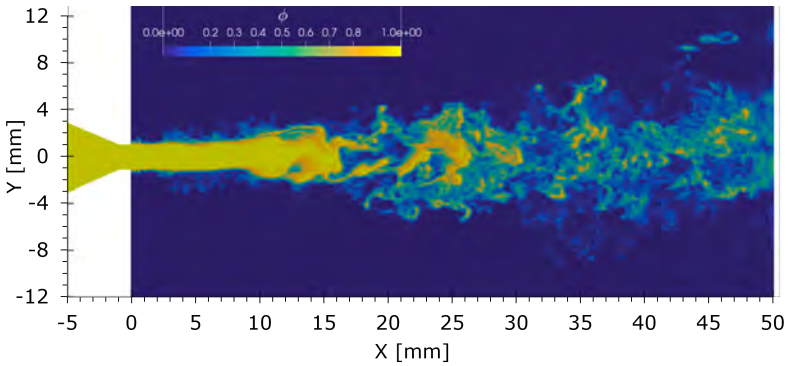

Figure 9: Liquid of volume fraction field.

liquid volume fraction ϕ=0.5 (Figure 10) where the droplet formation also occurs near the nozzle exit and in the presence of the liquid core. From the atomization point of view, it is around 12D to 18D where the primary break-up occurs and the liquid core is broken and where the extraction of liquid to compute droplets is obtained. These simulations will be used to obtain droplet statistics during continuous operation that can be used as boundary conditions of the Euler-Lagrange simulations. This is explained in the next subsection.

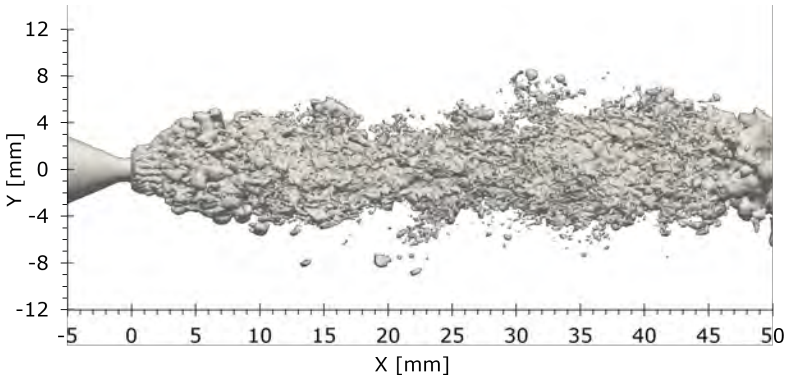

Figure 10: Iso-contour of liquid volume fraction ϕ=0.5

4.1.3. Phenomenological model for primary breakup

The two–phase LES model introduced in the previous sections can be used to provide a detailed description of the atomization process. This information

is employed to develop a phenomenological model for primary breakup that is used as a boundary condition of the spray injection for the Euler–Lagrange simulations.

The development of this phenomenological model is based on a two-step strategy. First, the two–phase Euler problem is solved in the computational domain and time-averaged quantities for the relevant parameters involved in the atomization process are obtained [21]. Second, a region describing the primary breakup is used to obtain statistics for particle size distributions and velocities.

The EE model provides the Sauter mean diameter (SMD) d_{32} as a computed quantity from the volume fraction and the interphase surface density, the mean SMD $< d_{32} >$ can be extracted after time-averaging the local SMD d_{32} during run-time.

For illustration, a snapshot of the SMD distribution in the computational domain at the steady condition is shown in Figure 11. High values of SMD are representative of the liquid core, where a low value indicates high atomization regions. As already mentioned, after the jet primary breakup, the surface region selected to obtain droplet statistics is ultimately defined by a threshold of the volume fraction, $\phi_0 = 0.1$. This is shown in Figure 12 and corresponds to values of $d_{32} = [10, 200]\,\mu m$ for our computational mesh.

Not only the SMD but also its distribution will be important in defining the appropriate boundary conditions for the LE model. Therefore, the probability density function (PDF) of the particle size distribution is shown in Figure 13. Finally, the distribution can be perfectly fitted by a Rosin–Rammler formula, that will be used with that SMD and the limits given the PDFs of the data.

After this analysis, the conclusion is that the LE spray injection conditions should be positioned in a location downstream from the primary breakup, which is around 1.4 cm (7D). From the experimental data, and confirmed by the numerical results, a spreading angle of 30 degrees is found for the liquid dispersion (confirming the manufacturer information [45]). Therefore, based on the numerical results and the statistical analysis, a circum-

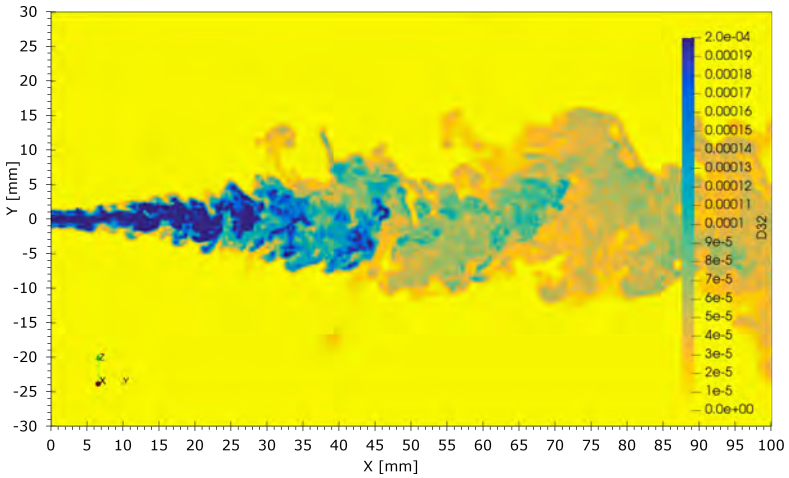

Figure 11: Distribution of SMD on a snapshot.

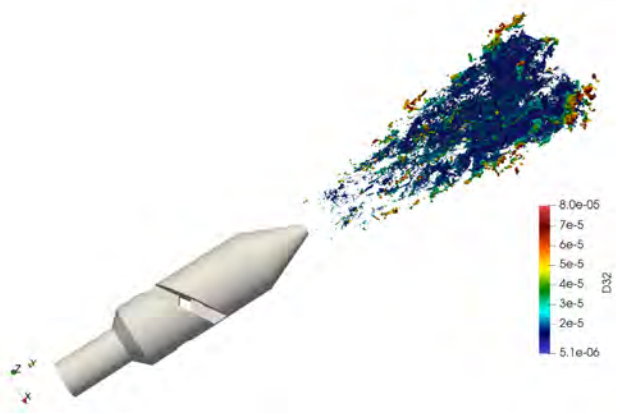

Figure 12: Primary breakup region extracted to compute particle size distribution statistics.

ferential injection with uniform particle distribution over the surface and a spreading angle of 30 degrees placed about 1.4 cm downstream the injection nozzle is proposed. The injection will be fed with particle sizes following the Rosin–Rammler distributions from Table 3 that match the corresponding flow rate.

Finally, the velocity of the particles needs to be defined. In this case, we extract a perpendicular plane to the flow normal direction and select the

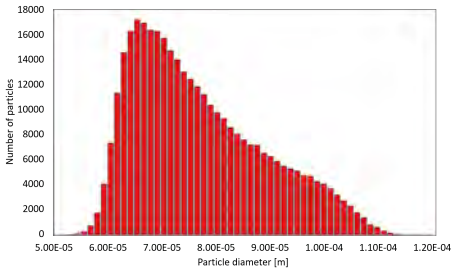

Figure 13: PDF of particle diameter

Flow rate	$d32\ [\mu m]$	$d_{min}\ [\mu m]$	$d_{max}\ [\mu m]$	$< U > \vert_{7D}\ [m/s]$	$d_e\ [mm]$
$\dot{m}_1$	70.0	30.0	90.0	12.630	5.65

Table 3: Phenomenological injection model based on a Rosin–Rammler distribution, effective diameter and particle average velocity

effective area corresponding to the nonzero axial velocity. Details of this process are shown in Figure 14. An averaged velocity for this effective area is computed and used, together with the effective diameter, to define the circumferential section where the inflow conditions are imposed.

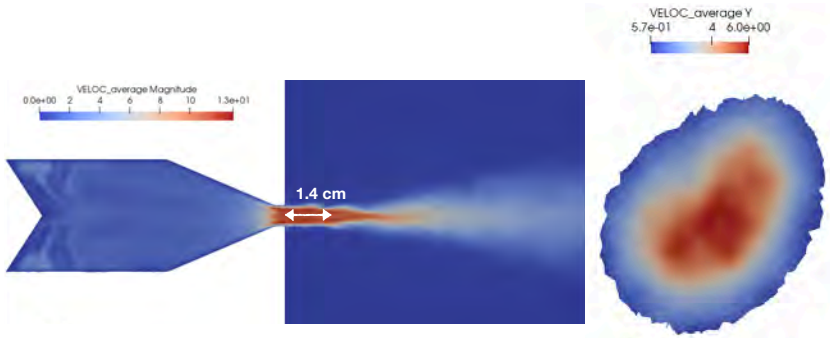

Figure 14: Average axial velocity with a mark of the primary breakup distance (left) and effect area for calculating average particle velocity (right)

The phenomenological model permits the generation of an accurate spray injection boundary condition for the Euler-Lagrange simulations and without the cost of rerunning Euler-Euler multiphase simulations.

4.2. Multiple droplet model (Euler-Lagrange)

In the previous section, a phenomenological model for the definition of an accurate spray injection model was described. The numerical solution is obtained with ANSYS–Fluent and compared with the experimental results.

The inputs of the Euler-Lagrange inflow boundary condition generator are defined using the methodology described in the previous section.

4.2.1. Numerical setup

The far field simulation focuses on the jet convection and the vaporization process solved with the EL model. The computational domain is a cylinder with a diameter of 2m and a height of 4m. An unstructured grid with around 30,000 elements is generated with ANSYS-Meshing module. This mesh was obtained from a grid convergence study done with three different grids. A refined area is considered to capture correctly the Eulerian solution (see Figure 15).

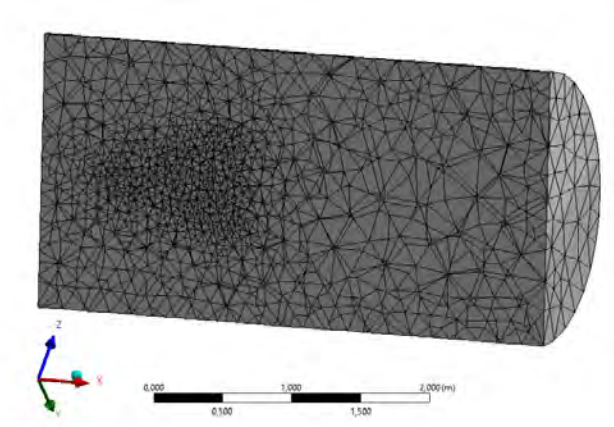

Figure 15: Cylindrical unstructured mesh section

The air is solved using the compressible Navier-Stokes equations. While the liquid droplets are tracked with the LPT approach described in Section 3.2.2. The LPT model includes a two–way coupling which is used to solve the droplet vaporization.

For the initial condition, the flow is considered at rest. Regarding the boundary conditions, the left wall (-x direction) is set as the velocity inlet

with zero velocity and the rest of the domain is set as the pressure outlet. The droplets are injected through a solid cone injection model using the velocity, mass flow rate, droplet size distribution, and spray angle from the EE simulation. The particles are able to escape from the domain. Finally, to ensure numerical stability, 25,000 particles per parcel are injected at each time step. The time step used for the simulation is 5E-5s.

4.2.2. Results

Particles distribution colored by diameter values are compared in Figure 16 (top) with DBI experimental results at steady state, where the evaporated particles are not visible. The spray angle of 30deg is well predicted (see view #1), this angle is loosed at a certain distance where the particles are evaporated (see view #2 and #4). Additionally, the numerical computation gives information about the distance where the Novec-1230 is completely evaporated. The vaporization distance is around 2m from the outlet nozzle.

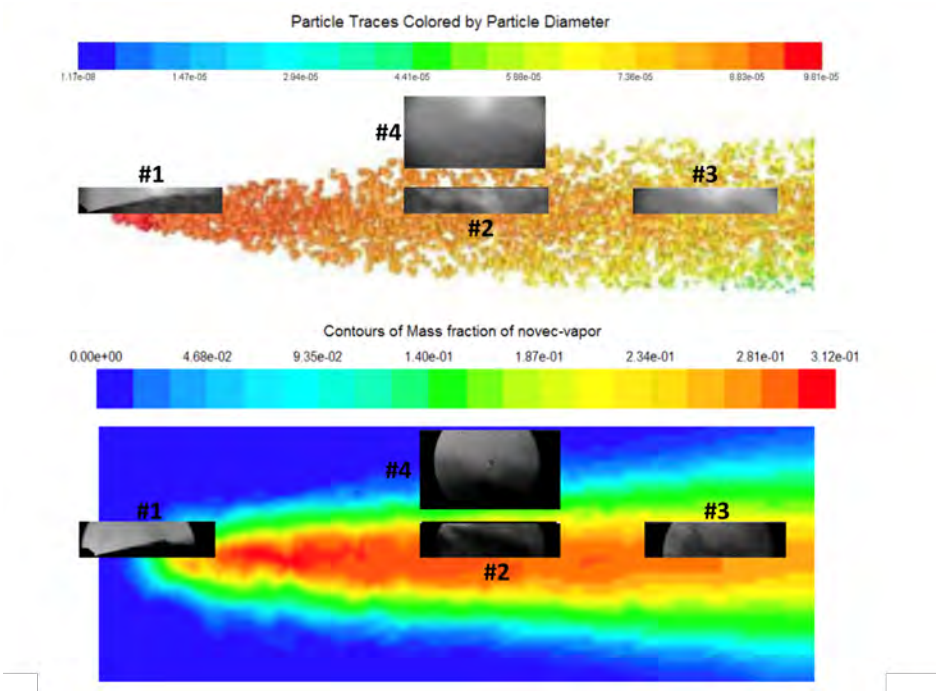

Figure 16: Comparison between ANSYS-Fluent Novec-1230 concentration and experimental results. DBI (top), Schlieren (bottom)

In contrast to the DBI comparison, Figure 16 (bottom) shows the Novec-1230 concentration in ANSYS-Fluent compared with Schlieren experimental results, where the density changes are captured. This comparison shows how the Novec-1230 evaporated maintain 30deg along the domain, which is captured by both the experimental and numerical results.

Finally, these results suggest that the liquid phase would reach distances of the order of 2 and 2.5 m with the use of this atomizer at the given flow rate, which is about the distance between the injector and the walls of the cargo hold in standard configurations. Therefore, different nozzle designs with larger spreading angles should be used instead to increase the effective area of Novec-1230 vapor and improve the distribution of the fire extinction agent in the cargo hold.

5. Parametric study

Once the methodology has been developed and validated with experimental data, different operating conditions can be simulated with the EL model saving computational effort compared with the EE model. The objective of this parametric study is to analyze the effect of the operating conditions (cargo hold pressure and temperature and Novec-1230 bottle temperature) into the vaporization of Novec-1230. Therefore, in this section, the unsteady RANS low–fidelity approach is used to simulate realistic operating conditions based on Arnav et al. work [7, 36]. The setup of the numerical experiment is identical to the one used in the previous section. In addition to the previous operating condition (see Section 2), two extra conditions have been included in this section. Table 4 shows the three realistic operating conditions. Conditions #1 and #2 represent a cabin altitude condition with (#1) and without (#2) thermal comfort in the cargo hold. Finally, condition #3 represents a ground condition (sea level) with warm temperature.

Table 5 shows the mass flow of Lagrangian particles (liquid Novec-1230) injected into the domain, and the mass flow of Novec-1230-vapor leaving the domain. Besides, the ratio between the liquid Novec-1230 injected into the domain and the Novec-1230-vapor leaving the domain is shown. If this value is close to 100% it means that most of the injected liquid Novec-1230

Condition	Cargo hold pressure [Pa]	Cargo hold temperature [K]	Novec-1230 bottle temperature [K]
#1	75000	288	273
#2	75000	268	248
#3	101325	298	318

Table 4: Operating conditions

evaporates within the CFD domain. As expected, the highest vaporization rate is obtained for the conditions #3 (78%), while lower vaporization rate is obtained for the condition of #2 (58%).

Condition	Lagrangian input [kg/s]	Novec-1230-vapor output [kg/s]	Novec-1230-vapor output/ Lagrangian input [%]
#1	0.235	0.163	69.4
#2	0.235	0.137	58.3
#3	0.235	0.183	77.8

Table 5: Operating conditions

Regarding the distribution of atomization, Figure 17 shows the Novec-1230-vapor concentration in the domain. It can be seen that the concentration is higher in the core of the atomization. Besides, the test with the higher temperature presents higher vaporization rates, as expected.

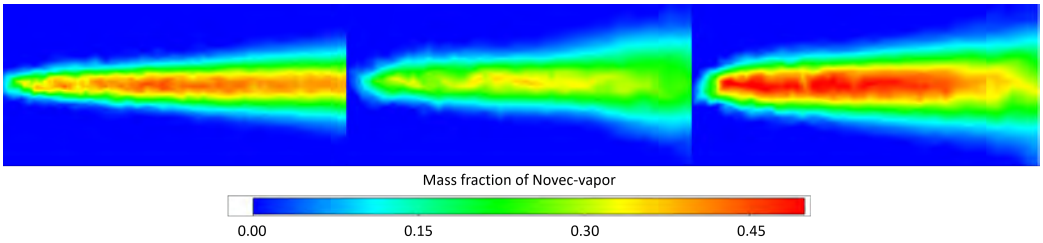

Figure 17: Mass fraction of Novec-1230-vapor at three different operating conditions, #1 (left), #2 (middle), and #3 (right)

6. Conclusions

In this work, we have presented a multi-scale methodology able to compute, at an affordable cost, the injection, dispersion, and vaporization of a liquid jet into quiescence air. This methodology is useful to generate accurate inflow boundary conditions for zonal models used in fire numerical simulations. The multi-scale approach entails two steps being the first one a high fidelity multiphase method and the second one a low fidelity particle-based method. This multi-scale approach requires a low number of High Performance Computing (HPC) level simulations coupled with a high number of simulations that are run in a workstation in ANSYS-Fluent.

For the near field (step one), the proposed approach studies the primary atomization of a liquid jet injected into the air using a high fidelity Large Eddy Simulation (LES) Euler-Euler model. It is based on an entropy stable conservative level set scheme stabilised with an entropy stable method for the regions where the interface can be resolved, while it includes a subgrid contribution when the slip velocity of the two-phase flow cannot be resolved with the given filter size. This model is implemented in the HPC simulation code ALYA. For the far field (step two), an Euler–Lagrange approximation is solved which includes a Eulerian description for the gas while the liquid is assumed to be dispersed and tracked as individual droplets. A two–way coupled model based on previous works in the simulation of fire suppression systems is used to solve the droplets vaporization in the Euler–Lagrange simulation. This model is implemented in ANSYS–Fluent.

This methodology has been applied to a generic fire suppression system, made of a nozzle which injects the agent (Novec-1230) into a large compartment. The results are compared with experimental data to show its validity. The validation shows that both the atomization and phase change processes are accurately captured by the proposed multi-scale methodology. Finally, a parametric study has been performed to show the qualitative trends of the variations of the operating conditions (cargo hold pressure and temperature and Novec-1230 bottle temperature) into the vaporization of Novec-1230.

Acknowledgement

This project has received funding from the European Union's Horizon 2020 research and innovation programme under the grant agreement No 785549 (FireExtintion: H2020-CS2-CFP06-2017-01).

References

[1] 3Mwebsite, 2020. URL: `http://www.3M.com/novec1230fluid`, Accessed: 2020-01-15.

[2] W. W. Jones, Review of Compartment Fire Models., Technical Report, 1983.

[3] J. Quintiere, A perspective on compartment fire growth, Combustion Science and Technology 39 (1984) 11–54.

[4] P. A. Reneke, R. D. Peacock, G. P. Forney, W. D. Davis, ZFM Zone Fire Model (Version 1) Reference Guide, Technical Report, 2017.

[5] G. Cox, Compartment fire modelling, Combustion fundamentals of fire (1995) 329–404.

[6] P. H. Thomas, The growth of fire-ignition to full involvement, Combustion fundamentals of fire (1995) 275–296.

[7] A. Pathak, V. Norrefeldt, M. Pschirer, Validation of a simulation tool for an environmentally friendly aircraft cargo fire protection system, Aerospace 8 (2021) 35.

[8] G. P. Forney, W. F. Moss, Analyzing and exploiting numerical characteristics of zone fire models, Fire Science and Technology 14 (1994) 49–60.

[9] V. Novozhilov, Computational fluid dynamics modeling of compartment fires, Progress in Energy and Combustion science 27 (2001) 611–666.

[10] S. Hoyas, A. Gil, X. Margot, D. Khuong-Anh, F. Ravet, Evaluation of the eulerian–lagrangian spray atomization (elsa) model in spray simulations: 2d cases, Mathematical and Computer Modelling 57 (2013) 1686–1693.

[11] G. Tryggvason, R. Scardovelli, S. Zaleski, Direct numerical simulations of gas–liquid multiphase flows, Cambridge University Press, 2011.

[12] C. W. Hirt, B. D. Nichols, Volume of fluid (VOF) method for the dynamics of free boundaries, Journal of computational physics 39 (1981) 201–225.

[13] M. Sussman, P. Smereka, S. Osher, et al., A level set approach for computing solutions to incompressible two-phase flow (1994).

[14] E. Olsson, G. Kreiss, A conservative level set method for two phase flow, Journal of computational physics 210 (2005) 225–246.

[15] D. Jacqmin, Calculation of two-phase Navier–Stokes flows using phase-field modeling, Journal of Computational Physics 155 (1999) 96–127.

[16] J. Manzanero, G. Rubio, D. A. Kopriva, E. Ferrer, E. Valero, A free–energy stable nodal discontinuous Galerkin approximation with summation–by–parts property for the Cahn–Hilliard equation, Journal of Computational Physics 403 (2020) 109072.

[17] J. Manzanero, G. Rubio, D. A. Kopriva, E. Ferrer, E. Valero, Entropy-stable discontinuous Galerkin approximation with summation-by-parts property for the incompressible Navier-Stokes/Cahn-Hilliard system, Journal of Computational Physics 408 (2020) 109363.

[18] M. Baer, J. Nunziato, A two-phase mixture theory for the deflagration to detonation transition (DDT) in reactive granular materials, International Journal of Multiphase Flow 12 (1986).

[19] F. Fraysse, C. Redondo, G. Rubio, E. Valero, Upwind methods for the Baer–Nunziato equations and higher-order reconstruction using artificial viscosity, Journal of Computational Physics 326 (2016) 805–827.

[20] J. D. Schwarzkopf, M. Sommerfeld, C. T. Crowe, Y. Tsuji, Multiphase flows with droplets and particles, CRC press, 2011.

[21] B. A. Vallet, A., R. Borghi, Development of a eulerian model for the atomization of a liquid jet, Atomization and sprays 11 (2001).

[22] G. Blokkeel, B. Barbeau, R. Borghi, A 3d eulerian model to improve the primary breakup of atomizing jet, SAE transactions (2003) 45–54.

[23] W. Ning, R. D. Reitz, A. M. Lippert, R. Diwakar, Development of a next-generation spray and atomization model using an Eulerian-Lagrangian methodology, Ph.D. thesis, University of Wisconsin–Madison, 2007.

[24] S. Hoyas, A. Gil, X. Margot, D. Khuong-Anh, F. Ravet, Evaluation of the Eulerian–Lagrangian Spray Atomization (ELSA) model in spray simulations: 2D cases, Mathematical and Computer Modelling 57 (2013) 1686–1693.

[25] J. Anez, A. Ahmed, N. Hecht, B. Duret, J. Reveillon, F. Demoulin, Eulerian–lagrangian spray atomization model coupled with interface capturing method for diesel injectors, International Journal of Multiphase Flow 113 (2019) 325–342.

[26] J.-L. Guermond, M. Q. de Luna, T. Thompson, An conservative anti-diffusion technique for the level set method, Journal of Computational and Applied Mathematics 321 (2017) 448–468.

[27] K. McGrattan, S. Hostikka, R. McDermott, J. Floyd, C. Weinschenk, K. Overholt, Fire dynamics simulator technical reference guide volume 1: mathematical model, NIST special publication 1018 (2013) 175.

[28] H. Mahmud, Simulation of the suppression of fires using water mists, Ph.D. thesis, Victoria University, 2016.

[29] J. Floyd, R. McDermott, Development and evaluation of two new droplet evaporation schemes for fire dynamics simulations, Fire Safety Journal 91 (2017) 643–652.

[30] M. Vázquez, G. Houzeaux, S. Koric, A. Artigues, J. Aguado-Sierra, R. Arís, D. Mira, H. Calmet, F. Cucchietti, H. Owen, et al., Alya: Multiphysics engineering simulation toward exascale, Journal of Computational Science 14 (2016) 15–27.

[31] A. Fluent, 18.0 ANSYS Fluent theory guide 18.0, Ansys Inc (2017).

[32] R. Payri, J. Gimeno, P. Martí-Aldaravi, C. Carvallo, Parametrical study of the dispersion of an alternative fire suppression agent through a real-size extinguisher system nozzle under realistic aircraft cargo cabin conditions, Process Safety and Environmental Protection 141 (2020) 110–122.

[33] R. Payri, F. J. Salvador, J. Gimeno, J. E. Peraza, Experimental study of the injection conditions influence over n-dodecane and diesel sprays with two ecn single-hole nozzles. part ii: Reactive atmosphere, Energy Conversion and Management 126 (2016) 1157–1167.

[34] J. V. Pastor, R. Payri, J. M. Garcia-Oliver, J.-G. Nerva, Schlieren measurements of the ECN-spray a penetration under inert and reacting conditions, Technical Report, SAE Technical Paper, 2012.

[35] D. Elliott, P. Garrison, G. Klein, K. Moran, M. Zydowicz, Flow of nitrogen-pressurized Halon 1301 in fire extinguishing systems (1984).

[36] Y. A. Cengel, et al., Air Transport Association Publications Spec (ATA-100), volume Chapter 21, 2000.

[37] F. De Lillo, M. Cencini, S. Musacchio, G. Boffetta, Clustering and turbophoresis in a shear flow without walls, Physics of Fluids 28 (2016) 035104.

[38] O. Lehmkuhl, D. Mira, L. Gasparino, H. Owen, G. Houzeaux, Large-eddy simulation of primary atomization using an entropy stable conservative level set, in: M. García-Villalba, H. Kuerten, M. V. Salvetti (Eds.), Direct and Large Eddy Simulation XII, Springer International Publishing, Cham, 2020, pp. 207–213.

[39] J. Chesnel, J. Reveillon, T. Menard, F.-X. Demoulin, Large eddy simulation of liquid jet atomization, Atomization and Sprays 21 (2011).

[40] A. Vreman, An eddy-viscosity subgrid-scale model for turbulent shear flow: Algebraic theory and applications, Physics of fluids 16 (2004) 3670–3681.

[41] S. Navarro-Martinez, Large eddy simulation of spray atomization with a probability density function method, International journal of multiphase flow 63 (2014) 11–22.

[42] O. Lehmkuhl, G. Houzeaux, H. Owen, G. Chrysokentis, I. Rodriguez, A low-dissipation finite element scheme for scale resolving simulations of turbulent flows, Journal of Computational Physics 390 (2019) 51–65.

[43] M. Farid, A new approach to modelling of single droplet drying, Chemical Engineering Science 58 (2003) 2985–2993.

[44] Y. A. Cengel, et al., Introduction to thermodynamics and heat transfer, volume 846, McGraw-Hill New York, 1997.

[45] Spraying systems co., 2020. URL: `https://www.spray.com/`, accessed: 2020-01-15.